



Research article

C–S couplings catalyzed by Ni(II) complexes of the type [(NHC)Ni(Cp)(Br)]



Eduardo Jaimes–Romano^a, Hugo Valdés^{b,*}, Simon Hernández–Ortega^a, Rosa Mollfulleda^b, Marcel Swart^{c,*}, David Morales–Morales^{a,*}

^aInstituto de Química, Universidad Nacional Autónoma de México, Circuito Exterior, Ciudad Universitaria, Coyoacán, Ciudad de México C.P. 04510, México

^bInstitut de Química Computacional i Catàlisi (IQCC) and Departament de Química, Universitat de Girona, Campus de Montilivi, Girona E–17003 Catalonia, Spain

^cInstitut de Química Computacional i Catàlisi (IQCC) & Departament de Química, Universitat de Girona, 17003 Girona, Spain ICREA, 08010 Barcelona, Spain

ARTICLE INFO

Article history:

Received 2 May 2023

Revised 2 July 2023

Accepted 3 July 2023

Available online 06 July 2023

Keywords:

C–S cross–coupling

Thioetherification reaction

NHC complexes

Nickel Catalysis

Thiolation reaction

Catalysis

ABSTRACT

The catalytic activities of three Ni(II) complexes with fluorinated and non–fluorinated N–heterocyclic carbene (NHC) ligands were evaluated in the C–S cross–coupling reaction between iodobenzene and thio–phenol. The complexes with fluorinated–NHC ligands exhibited lower catalytic activities compared to the non–fluorinated derivative. This can be attributed to the lower electron–donating character of the fluorinated ligands in comparison to the non–fluorinated ligand. Complex **3–Ni** was tested towards different substrates, achieving moderate to good conversions. Additionally, the reaction mechanism of the C–S cross–coupling using two substrates, tert–butylthiol and 2,4–dichlorobenzenethiol, was determined. Tert–butylthiol produced a stable intermediate that inhibited the last step of the reaction mechanism (reductive elimination). On the other hand, 2,4–dichlorobenzenethiol formed a less stable intermediate, favoring the reductive elimination. This observation aligns with the lower yield observed when using tert–butylthiol compared to 2,4–dichlorobenzenethiol (20% vs 99%).

© 2023 The Author(s). Published by Elsevier Inc. This is an open access article under the CC BY–NC–ND license (<http://creativecommons.org/licenses/by-nc-nd/4.0/>).

1. Introduction

N–heterocyclic carbene (NHC) ligands have been extensively studied in organometallics and catalysis over the last two decades for the design of highly catalytically active species in processes such as cross–coupling, metathesis, dehydrogenation, hydrogenation, and other industrially relevant reactions.[1–27] Their wide applicability is mainly due to their facile preparation and tunability, forming very strong σ bonds with practically any transition metal. However, their use in C–S cross–coupling has been scarcely explored, even though this transformation promises to be a greener route for the formation of C–S bonds, which are widely found in important biological and pharmaceutical products, such as nelfinavir, vortioxethine, etcetera.[28–31] Thus, C–S bond formation has become one of the most important targets in modern organic synthesis.

Some examples of Pd(II), Cu(I) and Ni(0/II) NHC complexes for C–S cross–couplings have been reported.[32–42] In the case of Ni–NHC catalysts, the focus has predominantly been on utilizing

imidazolyliene derivatives to generate the catalytically active species. In 2007, Zhang and Ying described a catalytic system based on Ni(0) and imidazolyliene ligands with N–benzyl substituents.[32] Subsequently, Nicasio and co–workers described a well–defined imidazolyliene–based Ni(II) complex.[34] The NHC ligand featured N–aryl substituents, while the metal center was coordinated with both an allyl and a chloride ligand. Jun and Lee supported imidazolyliene–Ni(II) complexes on magnetite/silica nanoparticles, facilitating their recycling and the purification of the products.[37] Puerta and Valerga reported the synthesis of a bidentate ligand incorporating imidazolyliene and pyridine moieties. The metal coordination sphere of the Ni(II) was completed by a cyclopentadienyl (Cp) ligand.[39] More recently, our group described the catalytic activity of well–defined Ni(II) complexes of the type [(NHC)Ni(Cp)(Br)], where the imidazolyliene ligand included a phthalimide moiety (Fig. 1).[41] In this study, we observed a trend: the more electron–donating the NHC ligand, the more active the produced catalyst. To tune the electronic properties of those NHC ligands,[43,44] we used different N–substituents i.e. –N^tBu, –NMe and –NBn. However, all yielded electron–donating effects and the influence of electron–withdrawing groups was not clear for the design of catalysts for C–S cross–coupling reactions.

* Corresponding authors.

E–mail addresses: hugo.valdes@udg.edu (H. Valdés), marcel.swart@udg.edu (M. Swart), damor@unam.mx (D. Morales–Morales).

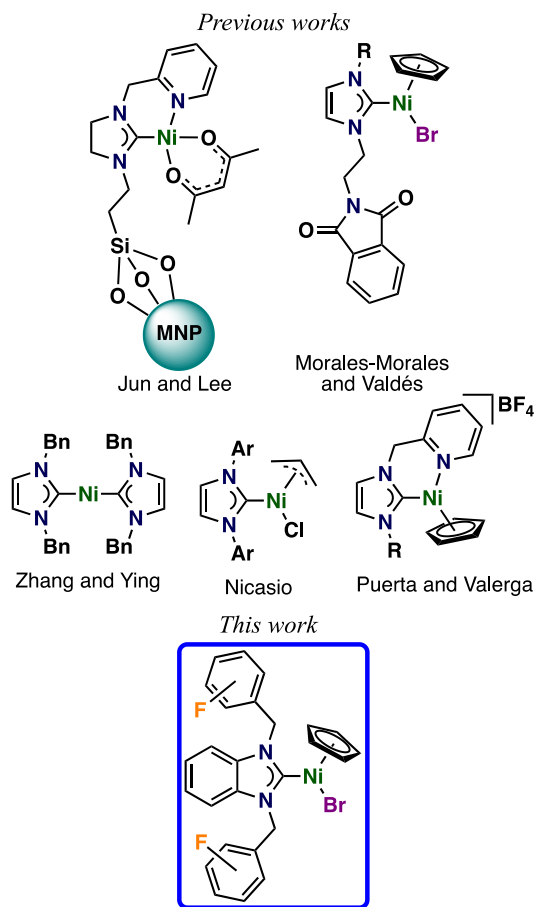


Fig. 1. Examples of NHC–Ni complexes used for C–S couplings.

Despite the existence of interesting examples of Ni(II)-based catalysts, the reaction mechanism of C–S cross-coupling has not been thoroughly investigated.[35,40,41] Sun and Zhou proposed a reaction mechanism involving three steps: oxidative addition, ligand exchange, and reductive elimination.[40] They also suggested that the catalytically active species is Ni(0), which can be formed through reductive elimination of the $[LNi(SR)_2]$ species, leading to the formation of $L-Ni(0)$ and $RS-SR$. The presence of $RS-SR$ was detected in the catalytic reaction mixture. However,

there is a lack of further experimental studies and theoretical calculations to support this proposed reaction mechanism.

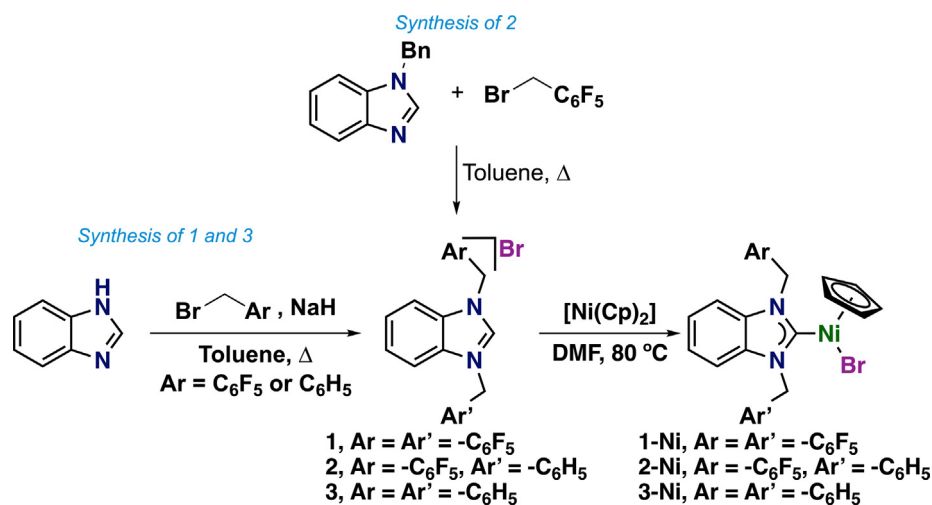
To further elucidate this topic, we conducted a study on the catalytic activities of three NHC complexes with clearly different electronic properties,[43,44] including N-substituents possessing electron-withdrawing properties. To achieve this, we employed both fluorinated and non-fluorinated N-benzyl groups (Fig. 1). Drawing from our previous research, we focused on complexes of the type $[(NHC)Ni(Cp)Br]$, with the NHC ligand being benzimidazolylidene. This ligand choice was based on its ability to generate more catalytically active complexes when compared to their imidazolylidene counterparts.[45] Furthermore, we evaluated the corresponding complexes in C–S cross-coupling reactions, and performed theoretical calculations to delve into the catalytic mechanism.

2. Results and discussion

We synthesized three benzimidazolium-based salts with different N-benzyl substituents: compound **1**, containing two perfluorinated benzyl fragments; compound **2**, comprising a non-fluorinated benzyl fragment and a perfluorinated benzyl fragment; and compound **3**, consisting of two non-fluorinated benzyl fragments. The synthesis of compounds **1** and **3** involved the reaction of benzimidazole with NaH and the respective benzyl bromide in refluxing toluene (Scheme 1). Compound **2** was prepared following a previously reported method.[46].

Next, we synthesized Ni(II) complexes of the type $[(NHC)Ni(Cp)(Br)]$ by reacting the corresponding azolium salt and $[Ni(Cp)_2]$ in DMF at 80 °C for 35 min (Scheme 1). After purification, complexes **1-Ni**, **2-Ni**, and **3-Ni** were obtained in yields of 65%, 52%, and 65%, respectively. Due to the diamagnetic nature of the Ni(II) complexes, they were amenable to be characterized by NMR spectroscopic techniques, characterization that was complemented with mass spectrometry, and elemental analyses.

The 1H NMR spectra of the complexes showed the absence of the signal corresponding to the proton $NCHN$, while a signal due to the presence of the Cp ligand was observed. Interestingly, this Cp signal was shifted downfield in the presence of the fluorinated-NHC ligands, following the trend **1-Ni** > **2-Ni** > **3-Ni** (5.42 > 5.27 > 5.12 ppm). DFT calculations at S12g/TZ2P level were also performed and supported this trend, with Cp values of 5.15 ppm (**1-Ni**), 5.00 ppm (**2-Ni**), 4.91 ppm (**3-Ni**). Similarly, in the ^{13}C $\{^1H\}$ NMR spectra the signals attributed to Cp displayed a similar



Scheme 1. Synthesis of Ni(II) complexes.

trend, 93.2 > 92.8 > 92.5 ppm, respectively. The corresponding calculated peaks appeared at 98.3 ppm (**1-Ni**), 97.7 ppm (**2-Ni**), 97.6 ppm (**3-Ni**). This trend was also observed for the characteristic $C_{\text{carbene-Ni}}$ signal, which appeared at 186.0 ppm for **1-Ni** > 183.9 ppm for **2-Ni** and 181.7 ppm for **3-Ni**. The computational data further confirmed this trend, with values of 210.6 ppm (**1-Ni**), 210.0 ppm (**2-Ni**), 208.9 (**3-Ni**). These findings are noteworthy, as the chemical shift of the carbene carbon is closely related with its electron-donating properties.[43,44] Hence, based on their structures, the NHC ligand with more fluorine atoms exhibited the least electron-donating character. Consequently, the NHC-Ni bond is weaker, resulting in an enhanced “free-NHC” character, and a downfield shift. This observation is consistent with the fact that the $^{13}\text{C}\{^1\text{H}\}$ NMR chemical shift of free-NHC ligands appears above 200 ppm, data that is further supported by DFT calculations (181.7 ppm).

Cyclic voltammetry studies were conducted on the three compounds to assess the electronics of the ligands (Fig. 2).[45] All compounds exhibited a one-electron reversible oxidation wave corresponding to a metal center redox process. To determine the half-wave potential of the complexes, differential pulse voltammetry (DPV) was employed. Complex **1-Ni** exhibited the highest potential (0.603 V), followed by **2-Ni** (0.590 V) and **3-Ni** (0.517 V). These values indicate that the presence of fluorine atoms decreases the electron-donating ability of the ligands on **1-Ni** and **2-Ni**. Conversely, the lower oxidation potential observed for **3-Ni** suggests a greater degree of electron-donating power of the non-fluorinated NHC ligand.

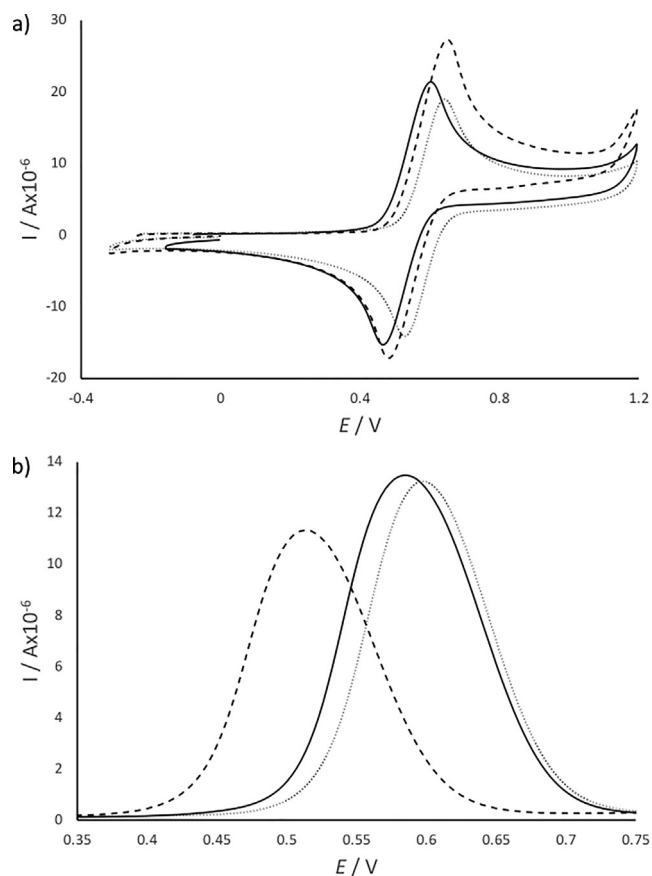


Fig. 2. A) cyclic voltammetry and b) differential pulse voltammetry of **1-Ni** (···), **2-Ni** (—) and **3-Ni** (---). The measurements were conducted in dry CH_2Cl_2 with 1 mM of analyte, using 0.1 M of $(\text{NBu}_4)\text{PF}_6$ as electrolyte, at a scan rate of $100 \text{ mV}\cdot\text{s}^{-1}$. The reference electrode was shifted to SCE by setting ferrocene at 440 mV.

The series of complexes were also analyzed by mass spectrometry analysis techniques (ESI⁺), resulting in clean spectra. For complex **1-Ni** the molecular ion $[\text{M}]^+$ was observed at 681.9 m/z , while for complexes **2-Ni** and **3-Ni** the molecular ions $[\text{M}-\text{Br}]^+$ were observed at 511.2 and 421.3 m/z , respectively. Moreover, crystals suitable for single crystal X-ray diffraction analysis were obtained for **1-Ni** and **3-Ni**, enabling the unequivocal determination of their molecular structures (Fig. 3). Both complexes exhibited an isostructural arrangement, showing the NHC ligand coordinated to the Ni center, with a bromide and a Cp ligand completing its coordination sphere. As expected, the metal center exhibited a ‘piano stool’ geometry. The Ni- C_{carbene} bond lengths for both complexes were very similar, 1.874(3) Å for **1-Ni** vs 1.872(3) Å for **3-Ni**. Our DFT studies showed similar bond-lengths with values of 1.848 Å (**1-Ni**), 1.846 Å (**2-Ni**) and 1.848 Å (**3-Ni**). The small variation in the Ni- C_{carbene} bond lengths may appear contradictory to the NMR and CV results, which indicate distinct electronic properties for the NHC ligands. However, the complexity of the Ni- C_{carbene} bond, particularly the interplay between σ -donation and π -back-donation properties of the carbenes, likely contributes significantly to the observed bond distances.[47].

With the complexes at hand, we studied their catalytic activities in C-S cross-coupling reactions. For this purpose, we monitored the progress of the catalytic reaction between iodobenzene and thiophenol in the presence of potassium *tert*-butoxide. The reactions were conducted using a 5 mol % catalyst loading in DMF at 100 °C (Fig. 4). As can be seen from the reaction profiles, the complex including the fluorinated NHC ligand (**1-Ni**) did not exhibit any activity throughout the process. In contrast, the complex with the non-fluorinated NHC ligand (**3-Ni**) displayed the highest activity, achieving an 89 % yield after 337 min, which corresponds to a TON of 18 and TOF of 3.2. As expected, the complex with a fluorinated N-substituent (**2-Ni**) was moderately active, affording a 40 % yield after the same reaction time. These findings agree well with the electronic character of the NHC ligands, whereby an increase in the electron-donating abilities of the NHC ligand leads to more active complexes. We have previously observed a similar trend under similar reaction conditions.[41] Moreover, we performed the mercury drop test and found no decrease in the reaction yield, suggesting that the reaction proceeds homogeneously.

The catalytic activity of complex **3-Ni** was good and comparable to that reported in the literature. For example, Zhang and Ying achieved a 99% yield of diphenylsulfane after 16 h using 1 mol% of their catalyst (Fig. 1), corresponding to a TON of 99 and a TOF of 6.2.[32] Nicasio and co-workers reported a 76% yield of diphenylsulfane after 24 h with their catalyst (TON = 76, TOF = 3.2), using NaO^tBu as the base and 1 mol% of catalyst.[34] Puerta and Valerga utilized 5 mol% of their catalyst and NaO^tBu , resulting in an 89% yield of diphenylsulfane after 24 h,[39] corresponding to a TON of 89 and a TOF of 0.7. In our previous work, the imidazolylidene-based Ni(II) complex reached a TON of 19 and a TOF of 38.4.[41] It is worth mentioning that these values were obtained by conducting the catalytic reaction under similar conditions, in DMF at 100 °C.

Encouraged by these results, we further explored the catalytic activity of complex **3-Ni** towards different thiol substrates, including aliphatic, aromatic, and heterocyclic derivatives (Table 1). Under similar reaction conditions, we observed low conversions when using aliphatic substrates. Interestingly, while using aliphatic substrates, we detected the formation of RS-SR product by GC-MS (see Supporting Information). This product can be formed through the coordination of two thiols to the nickel center, followed by reductive elimination (*vide infra*). In contrast, thiophenol derivatives showed conversions of up to > 99. The catalytic performance was influenced by the nature and position of substituent

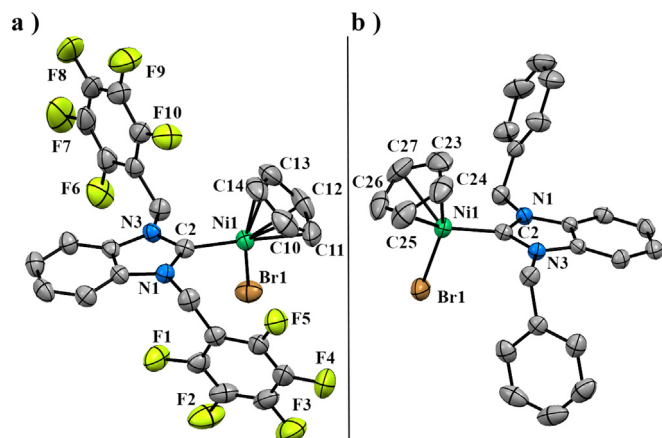


Fig. 3. Molecular structures of a) **1-Ni** and b) **3-Ni**. The ellipsoids are represented at 50% probability and hydrogen atoms were omitted for clarity. Selected bond lengths (Å): **1-Ni** = Ni(1)–C(2) 1.874(3), Ni(1)–Br(1) 2.3319(5). **3-Ni** = Ni(1)–C(2) 1.872(3), Ni(1)–Br(1) 2.3240(6).

groups. For instance, when a fluorine atom is at the *para*- or *meta*-position the conversions were of 68 and 58%, however using the *meta*-derivative produced no conversion at all. Interestingly, the highly electron-withdrawing group $-\text{CF}_3$ located at the *meta*-position produces a conversion of 94% (Entry 11, Table 1), but when located at the *para*-position the conversion reaches only 39% (Entry 10, Table 1). Unfortunately, catalyst **3-Ni** failed to produce the expected C–S coupling products for certain heterocyclic-thiol substrates (Entries 14–15, Table 1). However, it displayed low activity towards 2-benzothiazolethiol (Entry 16, Table 1).

Once we completed the evaluation and exploration of the C–S couplings, we proceeded to investigate the reaction mechanism through DFT calculations. Our hypothesis is that the mechanism follows three main steps: oxidative addition, ligand exchange, and reductive elimination. Similar to other cross-coupling reactions, we anticipated that metals in a low oxidation state would perform the oxidative addition. Therefore, we proposed that the Ni(II) is reduced to Ni(0). Considering the formation of a disulfur compound, we proposed that two thiolate ligands coordinate to the metal center. Subsequently, through a reductive elimination process, the disulfur compound and the Ni(0) species are formed. To facilitate the coordination of the two thiolate ligands, we suggest that the Cp ligand undergoes protonation.

Previous to perform the DFT calculations (*vide infra*) to support our hypothesis, we investigated the formation of four possible rotamers of complex **3-Ni** (Fig. 5). This analysis was conducted because these rotamers could potentially stabilize some of the catalytic intermediate species. The presence of N-benzyl substituents on the NHC ligand allows for flexibility and rotation around the C–N bond. Consequently, at each point along the reaction pathway, there could be four potential orientations of the phenyl groups: both phenyl groups oriented upwards (+z; *syn* to Cp) or downwards (–z; *anti* to Cp) when the NHC backbone is in the *xy*-plane; i.e. in isomer **a**, both phenyls are *syn* to Cp, while in isomer **b**, both are *anti* to Cp. Isomers **c** exhibit one phenyl group in the *syn* orientation and one phenyl in the *anti* orientation. In the X-ray structures (*vide supra*), these phenyl groups were observed as *anti-syn* (**c'** for **1-Ni** and **c** for **3-Ni**) but a rotational energy profile at S12g/TZ2P level showed that the rotational barriers are in general low, in the order of 5–6 kcal·mol^{–1}. Interestingly, the preferred orientation of the aromatic rings changed along the C–S cross-coupling reaction pathway (*vide infra*), rearranging between *syn-syn*, *anti-syn* and *anti-anti*, as the reaction proceeds.

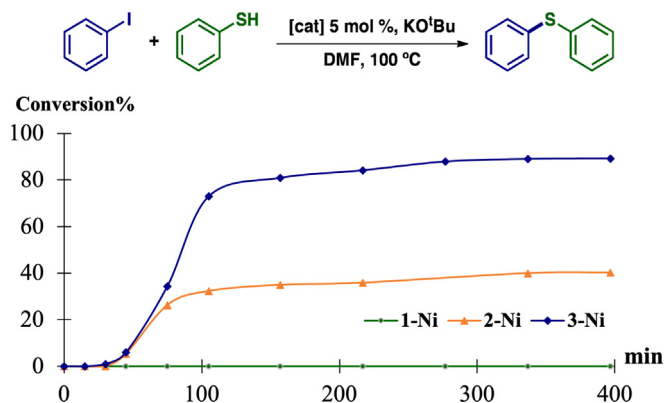


Fig. 4. Time-course reaction profiles for the reaction of iodobenzene and thiophenol. Reaction conditions: iodobenzene (0.25 mmol), thiophenol (0.25 mmol), KO^tBu (0.25 mmol) and [cat] (5 mol %) in DMF (3 mL) at 100 °C.

To gain insight into the influence of electron-withdrawing substituents on the reaction mechanism (Fig. 6), we conducted a computational study of the reaction mechanism with two substrates: *tert*-butylthiol (Fig. 7) and 2,4-dichlorobenzenethiol (Fig. 8). In the proposed mechanism depicted in Fig. 6, the reaction starts from complex I, and during the transition state, a reductive elimination takes place, leading to the release of *tert*-butyl disulfide, and the reduction of nickel to complex II Ni(0), which then serve as the starting point for the catalytic cycle with two available coordination sites. It is noteworthy the fact that *tert*-butyl disulfide was experimentally observed in the catalytic reaction. This is followed by the oxidative addition of aryl iodide; oxidizing this nickel species to complex III, a Ni(II) compound. The next transition state occurs in two steps, first the iodide is released, forming a reaction intermediate and then the thiolate is incorporated into the molecule to form complex IV. Finally, a reductive elimination occurs, where the C–S bond is formed, releasing the final product and starting the cycle once again with the initial complex II.

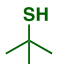
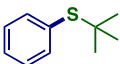
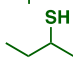
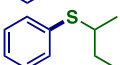
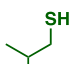
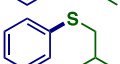
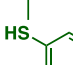
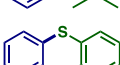
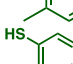
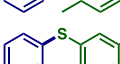
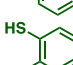
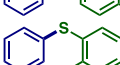
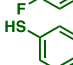
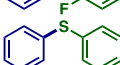
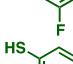
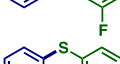
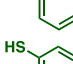
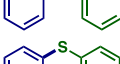
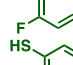
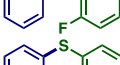
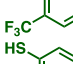
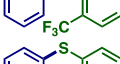
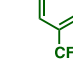
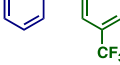
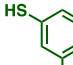
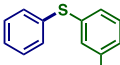
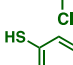
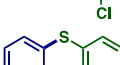
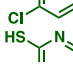
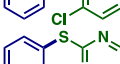
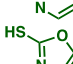
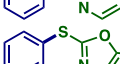
By comparing the free energy profiles of the two substrates (Fig. 9), we found that complex IV showed the highest energetic difference. *Tert*-butylthiolate forms a more stable complex than 2,4-dichlorobenzenethiolate, so the reductive elimination requires more energy using the alkyl-thiolate than the aromatic thiolate. Thus, the formation of the final product demands a higher amount of energy (~8.5 kcal·mol^{–1}), which justifies the difference in the yields obtained experimentally: 20% for *tert*-butylthiol vs 99% for 2,4-dichlorobenzenethiol.

3. Conclusion

In conclusion, we have prepared three Ni complexes of the type [(NHC)Ni(Cp)(Br)], two of them including fluorinated-NHC ligands. The complexes were characterized through NMR spectrometry, mass spectrometry, elemental analysis, and computational chemistry. The molecular structures of two complexes were determined unambiguously by single crystal X-ray diffraction analysis, and confirmed by DFT.

The catalytic performance of the three complexes was determined in the C–S cross-coupling of benzenethiol and iodobenzene, being the most active catalyst the non-fluorinated complex **3-Ni**, while the perfluorinated complex **1-Ni** was inactive in this transformation. This simple comparative study allows us to determine that the higher the electron-donating character of the NHC ligand is, leads to a higher catalytic activity of the complex. These results

Table 1
Cross-couplings between iodobenzene and different thiols catalyzed by 3-Ni.^a

Entry	Substrate (HS-R)	Product	Conversion (%) ^b	Turnover number (TON) ^c	Turnover frequency (TOF) ^d
1			20	4	0.2
2			0.0	0	0.0
3			16	3	0.2
4			88	18	0.9
5			57	11	0.6
6			68	14	0.7
7			0.0	0	0.0
8			58	12	0.6
9			71	14	0.7
10			39	8	0.4
11			94	19	1.0
12			36	7	0.4
13			>99	20	1.0
14			0.0	0	0.0
15			0.0	0	0.0
16			26	5	0.3

[a] Reaction conditions: iodobenzene (0.25 mmol), thiol (0.25 mmol), KO^tBu (0.25 mmol) and [cat] (5 mol %) in DMF (3 mL), 100 °C for 19 h. [b] Conversions obtained by GC-MS are based on residual iodobenzene and are the average of two runs. [c] TON = number of moles of product / number of moles of catalyst. [d] TOF = TON / reaction time (h).

are important and must be considered for the design of future catalyst for this important C–S cross-coupling reaction.

A mechanistic hypothesis consistent with the experimental and computational results is illustrated in Fig. 6. The hypothesis elucidates the feasibility of each step of the reaction, considering different conformations. Moreover, the nucleophilic character of the thiol emerges as a crucial factor influencing the catalytic performance. Highly nucleophilic thiols, such as tert-butylthiol, facilitate the stabilization of the last intermediate (intermediate IV) in the catalytic cycle. This additional stabilization prevents the reductive elimination step, resulting in the quenching of the C–S cross-coupling reaction, and consequently leading to low yields. In contrast, the utilization of less nucleophilic thiols, such as aromatic thiols

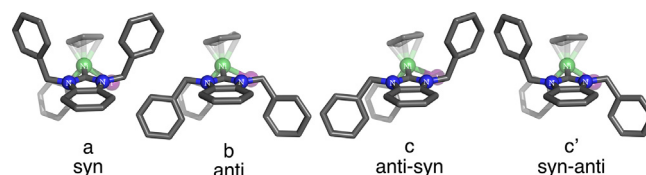


Fig. 5. Orientations of the N-benzyl group.

like 2,4-dichlorobenzenethiol, reduces the energy requirement for reductive elimination. Consequently, the C–S cross-coupling reaction becomes feasible, leading to higher yields.

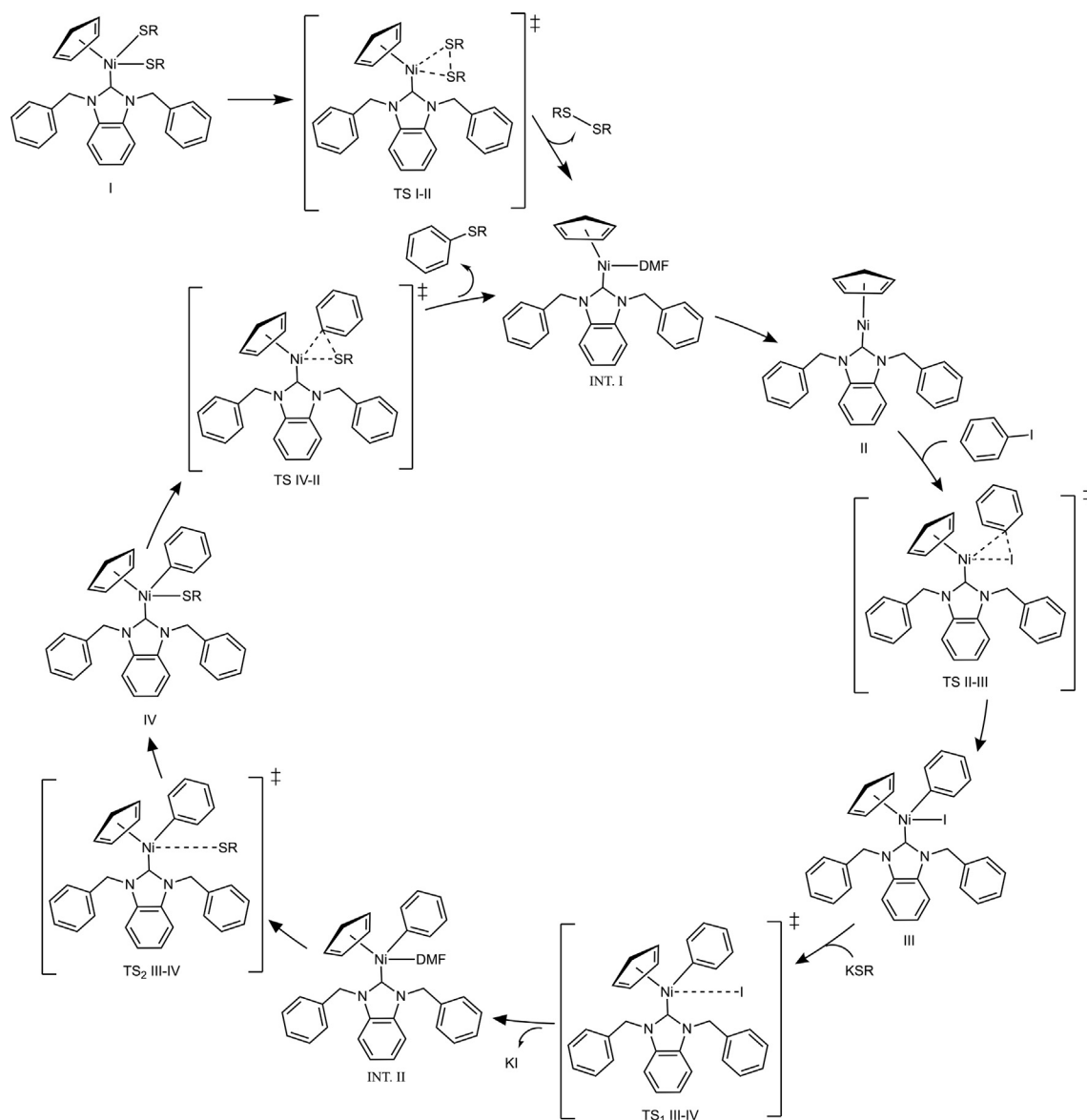


Fig. 6. Transition states of the reaction mechanism.

4. Experimental section

4.1. Materials

All reactions were carried out under nitrogen with standard Schlenk techniques unless otherwise stated. All chemical compounds were commercially obtained from Aldrich Chemical Co. and used as received without further purification. The azolium salt **2** was prepared according to the literature.[46] The ^1H and $^{13}\text{C}\{^1\text{H}\}$ NMR spectra were recorded on a Bruker Ascend 500 spectrometer or on a JEOL GX300 spectrometer. Chemical shifts are reported in ppm down field of TMS using the residual signals in the solvent as internal standard. Elemental analyses were performed on a Perkin Elmer 240. MS–Electrospray determinations were recorded on a Bruker Daltonics–Esquire 3000 plus Electrospray Mass Spectrometer. Mass measurements in FAB^+ were performed at a resolution of 3000 using magnetic field scans and the matrix ions as the reference material or, alternatively, by electric field scans with the

sample peak bracketed by two (polyethylene glycol or cesium iodide) reference ions. CV and DPV experiments were conducted using a CH Instrument Potentiostat model CHI620D. The cell was equipped with platinum working and counter electrodes, as well as a silver wire reference electrode. In all experiments, $[\text{NBu}_4][\text{PF}_6]$ (0.1 M in dry CH_2Cl_2) was used as the supporting electrolyte with an analyte concentration of approximately 1 mM. Measurements were performed at scan rates of 50 and 100 mV/s^{-1} . All redox potentials were referenced to the Fc^+/Fc couple as an internal standard, with $E_{1/2}(\text{Fc}/\text{Fc}^+) \text{ vs. SCE} = +0.44 \text{ V}$.

4.2. General procedure for the synthesis of the azolium salts

A solution of benzimidazole (474 mg, 4.0 mmol) and NaH (144 mg, 6.0 mmol) in toluene (10 mL) was stirred at room temperature for 10 min. Then, the corresponding benzyl bromide (11 mmol) was added to the solution. The resulting solution was heated to reflux for 12 h. After this time, the solution was allowed

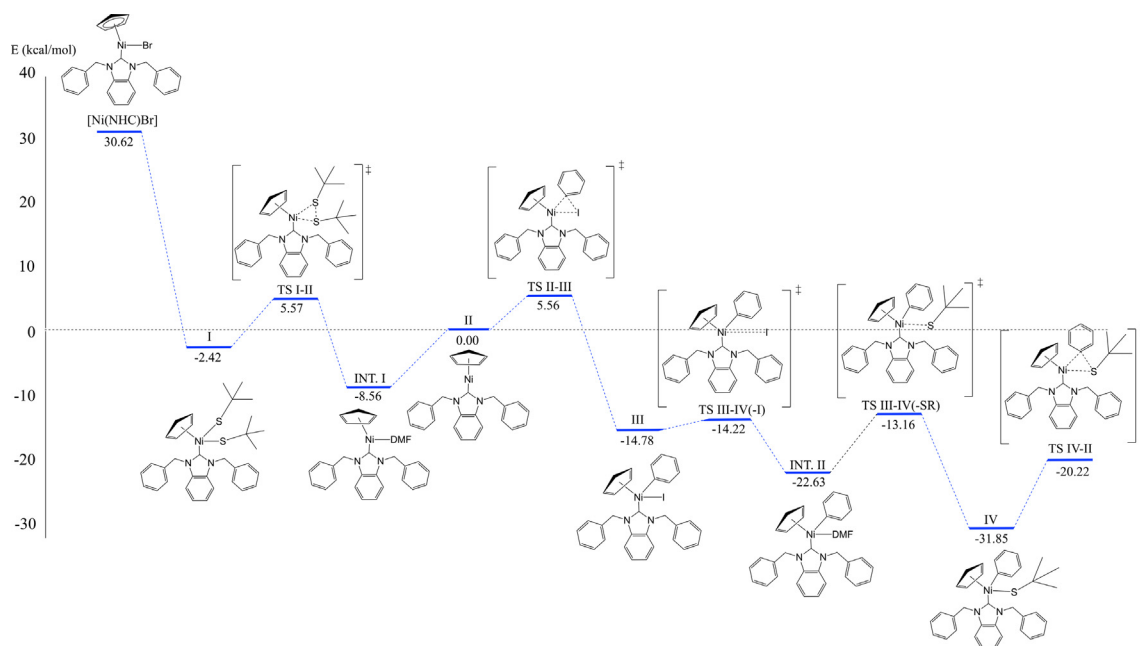


Fig. 7. Free energy profile of the C–S cross-coupling using tert-butylthiol.

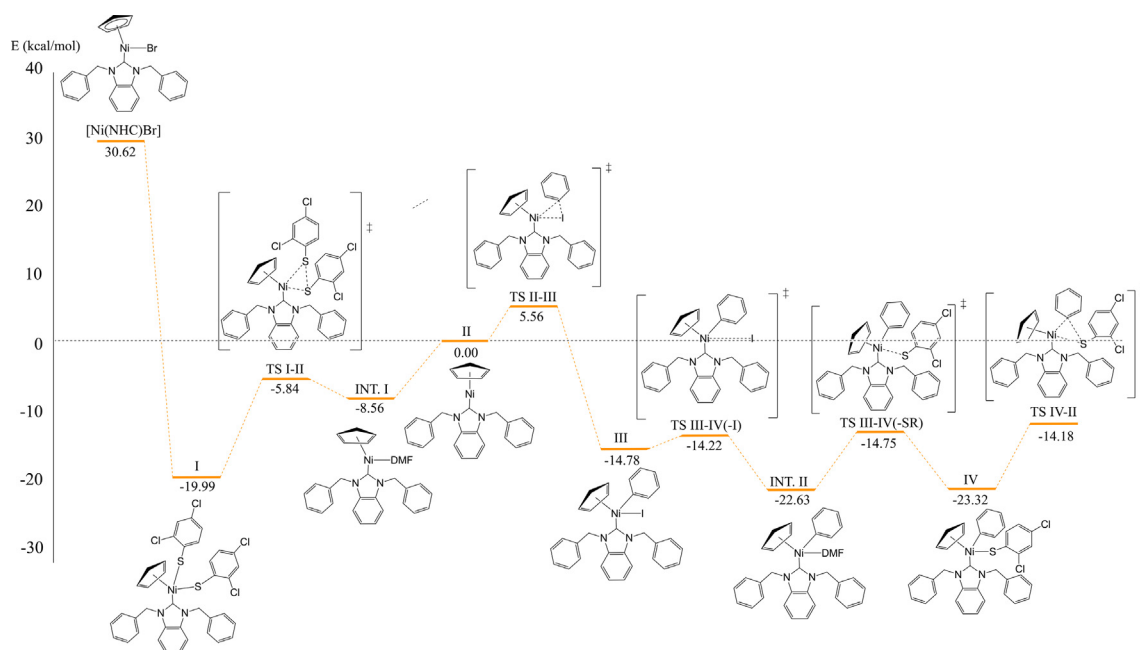


Fig. 8. Free energy profile of the C–S cross-coupling using 2,4-dichlorobenzenethiol.

to cool down to room temperature and filtered. The white solid was triturated in CH_2Cl_2 (100 mL) and filtered through celite[®]. The solution was concentrated under high vacuum to afford a white solid that contained the desired product.

4.2.1. Azolium salt (1)

The synthesis of **1** was carried out using 2,3,4,5,6-pentafluorobenzyl bromide (1.7 mL, 11 mmol). Yield: 2.1 g (81 %). ^1H NMR (301 MHz, CDCl_3) δ 11.41 (s, 1H, NCHN), 7.86 – 7.55 (m, 4H,

CHBIm), 6.23 (s, 4H, $-\text{CH}_2-$). $^{13}\text{C}\{^1\text{H}\}$ NMR (76 MHz, CDCl_3) δ 147.3 – 147.3 (m, CF_{Arom}), 144.1 (NCHN), 144.0 – 143.6 (m, CF_{Arom}), 141.1 – 140.4 (m, CF_{Arom}), 139.8 – 139.8 (m, CF_{Arom}), 136.2 – 136.2 (m, CF_{Arom}), 130.7 (C_{BIm}), 128.3 (CH_{BIm}), 113.0 (CH_{BIm}), 106.7 – 106.6 (m, C_{Arom}), 39.7 ($-\text{CH}_2-$). $^{19}\text{F}\{^1\text{H}\}$ NMR (283 MHz, CDCl_3) δ –140.2 (d, $J = 15.1$ Hz), –149.7 (t, $J = 21.0$ Hz), –158.8 – –159.6 (m). MS (IE^+) m/z 479.06 $[\text{M}-\text{Br}]^+$. Elem. Anal. Calcd. for $\text{C}_{21}\text{H}_9\text{F}_{10}\text{N}_2\text{Br}$: C, 50.64; H, 2.68; N 4.35. Found: C, 50.60; H, 2.66; 4.31.

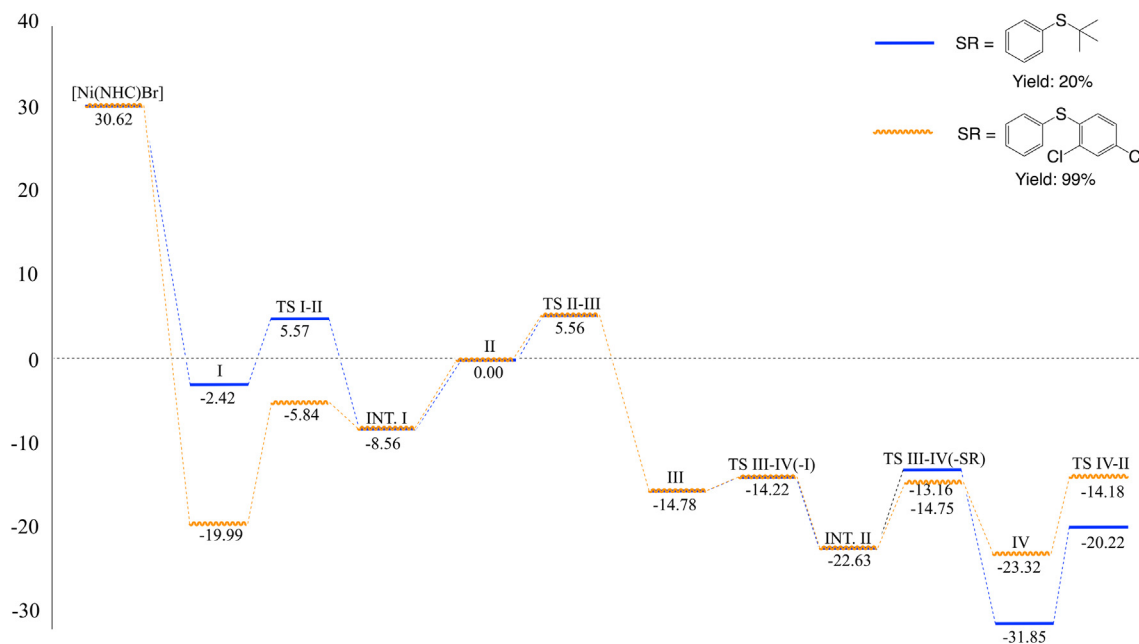


Fig. 9. Free energy profile of the C–S cross-coupling: tert-butylthiol (blue line) vs 2,4-dichlorobenzenethiol (red line). (For interpretation of the references to color in this figure legend, the reader is referred to the web version of this article.)

4.2.2. Azolium salt (3)

The synthesis of **3** was carried out using benzyl bromide (1.3 mL, 11 mmol). Yield: 0.9 g (60 %). The spectroscopic data were similar to those previously reported in the literature.[48].

4.3. General procedure for the synthesis of NHC–Ni(II) complexes

A solution of $[\text{Ni}(\text{Cp})_2]$ (100 mg, 0.5 mmol) and the corresponding azolium salt (0.2 mmol) in DMF was heated at 80 °C. After 30–40 min the color of the solution changes from dark green to red. After this time, the solution was cooled to room temperature and all the volatiles were removed under high vacuum. The crude solid residue was dissolved in CH_2Cl_2 (1 mL) and purified by column chromatography using silica gel. Elution with CH_2Cl_2 afforded the separation of a red band that contained the desired complex.

4.3.1. Complex (1–Ni)

The synthesis of complex **1–Ni** was carried out using azolium salt **1** (127.9 mg, 0.2 mmol). Yield: 89 mg (65 %). ^1H NMR (301 MHz, CDCl_3) δ 7.44 – 6.94 (m, 6H, $-\text{CH}_2-$ (2) and CH_{BIm} (4)), 5.97 (d, $J = 16.0$ Hz, 2H, $-\text{CH}_2-$), 5.42 (s, 5H, CH_{Cp}). $^{13}\text{C}\{^1\text{H}\}$ NMR (76 MHz, CDCl_3) δ 186.0 (Ni– $\text{C}_{\text{carbene}}$), 147.9 – 146.5 (m, C_{Arom}), 144.8 – 142.6 (m, C_{Arom}), 140.2 – 138.6 (m, C_{Arom}), 136.8 – 135.9 (m, C_{Arom}), 135.0 (C_{BIm}), 123.7 (CH_{BIm}), 110.0 (CH_{BIm}), 109.7 – 108.3 (m, C_{Arom}), 93.2 (CH_{Cp}), 43.7 ($-\text{CH}_2-$). MS (ESI⁺): m/z 681.9 $[\text{M}]^+$. Elem. Anal. Calcd. for $\text{C}_{26}\text{H}_{13}\text{BrF}_{10}\text{N}_2\text{Ni}$: C, 45.79; H, 1.92; N, 4.11. Found: C, 45.72; H, 1.84; N, 4.06.

4.3.2. Complex (2–Ni)

The synthesis of complex **2–Ni** was carried out using azolium salt **2** (93.8 mg, 0.2 mmol). Yield: 62 mg (52 %). ^1H NMR (301 MHz, CDCl_3) δ 7.50 – 7.24 (m, 4H, $-\text{CH}_2-$ (1) and CH_{Arom} (3)), 7.24 – 6.97 (m, 6H, CH_{BIm} (4) and CH_{Arom} (2)), 6.89 (d, $J = 15.9$ Hz, 1H, $-\text{CH}_2-$), 6.19 – 5.86 (m, 2H, $-\text{CH}_2-$), 5.27 (s, 5H, CH_{Cp}). $^{13}\text{C}\{^1\text{H}\}$ NMR (76 MHz, CDCl_3) δ 183.9 (Ni– $\text{C}_{\text{carbene}}$), 144.7 – 143.7 (m, C_{Arom}), 137.1 – 135.0 (m, C_{Arom}), 129.2 (CH_{Arom}), 128.1 (C_{BIm}), 126.4 (CH_{Arom}), 123.4 (CH_{BIm}), 111.2 (C_{Arom}), 109.6 (CH_{BIm}), 92.8 (CH_{Cp}), 54.0 ($-\text{CH}_2-$), 43.6 ($-\text{CH}_2-$). MS (ESI⁺): m/z

511.2 $[\text{M} - \text{Br}]^+$. Elem. Anal. Calcd. for $\text{C}_{26}\text{H}_{18}\text{BrF}_5\text{N}_2\text{Ni}$: C, 52.75; H, 3.06; N, 4.73. Found: C, 52.86; H, 3.16; N, 4.63.

4.3.3. Complex (3–Ni)

The synthesis of complex **3–Ni** was carried out using azolium salt **3** (75.9 mg, 0.2 mmol). Yield: 65 mg (65%). ^1H NMR (301 MHz, CDCl_3) δ 7.50 – 7.32 (m, 6H, CH_{Arom}), 7.32 – 7.27 (m, 4H, CH_{Arom}), 7.11 (s, 4H, CH_{BIm}), 6.93 (d, $J = 16.2$ Hz, 2H, $-\text{CH}_2-$), 6.18 (d, $J = 16.2$ Hz, 2H, $-\text{CH}_2-$), 5.16 (s, 5H, CH_{Cp}). $^{13}\text{C}\{^1\text{H}\}$ NMR (76 MHz, CDCl_3) δ 181.7 (Ni– $\text{C}_{\text{carbene}}$), 136.2 (C_{Arom}), 135.7 (C_{BIm}), 129.2 (CH_{Arom}), 128.1 (CH_{Arom}), 126.7 (CH_{Arom}), 123.0 (CH_{BIm}), 110.9 (CH_{BIm}), 92.5 (CH_{Cp}), 54.0 ($-\text{CH}_2-$). MS (ESI⁺): m/z 421.3 $[\text{M} - \text{Br}]^+$. Elem. Anal. Calcd. for $[\text{C}_{26}\text{H}_{23}\text{N}_2\text{BrNi}]$: C, 62.20; H, 4.62; N, 5.58. Found: C, 61.98; H, 4.67; N, 5.60.

4.4. General procedure for the C–S cross-coupling

Under inert atmosphere of nitrogen, a solution of KO^tBu (0.25 mmol) and the corresponding catalyst (5 mol %) in DMF (3 mL) was stirred at room temperature for 10 min. Then, iodobenzene (0.25 mmol) and the respective thiol (0.25 mmol) were added to the solution. The reaction was heated at 100 °C for the desired time. The reaction mixture was cooled to room temperature and the organic phase analyzed by gas chromatography (GC–MS) (Quantitative analyses were performed on an Agilent 6890 N GC with a 30.0 m DB–1MS capillary column couple to an Agilent 5973 Inert Mass Selective detector).

4.5. Data collection and refinement for compound (1–Ni) and (3–Ni)

Crystals of **1–Ni** (CCDC 2061468) and **3–Ni** (CCDC 2061469) were grown by slow diffusion of *n*-hexane into a saturated solution of the corresponding compound in CH_2Cl_2 . The crystals were mounted on glass fibers, then placed on a Bruker Smart Apex II diffractometer with a Mo–target X-ray source ($\lambda = 0.71073$ Å). The detector was placed at a distance of 5.0 cm from the crystals and frames were collected with a scan width of 0.5 in ω and an exposure time of 10 s/frame. Frames were integrated with the Bru-

ker SAINT software package[49] using a narrow-frame integration algorithm. Non-systematic absence and intensity statistics were used in monoclinic C2/c and monoclinic P2/c space groups respectively. The structures were solved using Patterson methods using SHELXS-2014/7 program.[50] The remaining atoms were located via a few cycles of least squares refinements and difference Fourier maps. Hydrogen atoms were input at calculated position and allowed to ride on the atoms to which they are attached. The final cycles of refinement were carried out on all non-zero data using SHELXL-2014/7.[50] Absorption corrections were applied using SADABS program.[51].

4.6. Computational details

To support the experimental results of the thioetherification reaction mechanism, we carried out the study of the possible energetic pathways of each reaction step, using density functional theory by means of the Amsterdam Density Functional (ADF) and QUILD programs. A triple- ζ valence basis set with double polarization functions (TZ2P) of Slater-type orbitals (STO) was used.[52,53] Relativistic corrections using the zero-order regular approximation (ZORA) combined with the S12g[54] density functional were used to calculate energies and gradients, which include the Grimme D3 dispersion model. The COSMO model for the solvent dimethylformamide (DMF) is included in which a dielectric continuum model of the solvent is taken into account. Note that both dispersion, solvation and relativistic effects were included self-consistently in all calculations. This method is suitable for nickel complexes, as shown in previous studies.[55,56].

4.7. Supplementary information

Supplementary data for compounds **1-Ni** and **3-Ni** was deposited at the Cambridge Crystallographic Data Centre. Copies of this information are available free of charge on request from The Director, CCDC, 12 Union Road, Cambridge, CB2 1EZ, UK (Fax: +44-1223-336033; e-mail deposit@ccdc.cam.ac.uk or www: <https://www.ccdc.cam.ac.uk>) quoting the deposition numbers 2061468–2061469.

All computational data have been uploaded (<https://doi.org/10.19061/iochem-bd-4-59>, link: <https://doi.org/10.19061/iochem-bd-4-59>) onto the IOCHEM-BD platform (<https://www.iochem-bd.org>) to facilitate data exchange and dissemination, according to the FAIR principles[57] of Open Data sharing.

Data availability

I have shared the link to my data at the Attach data step

Declaration of Competing Interest

The authors declare that they have no known competing financial interests or personal relationships that could have appeared to influence the work reported in this paper.

Acknowledgements

We would like to thank Dr. Francisco Javier Pérez Flores, Q. Eréndira García Ríos, M.Sc. Lucía del Carmen Márquez Alonso, M. Sc. Lucero Ríos Ruíz, M.Sc. Alejandra Núñez Pineda (CCIQS), Q. María de la Paz Orta Pérez, Q. Roció Patiño-Maya and Ph.D. Nuria Esturau Escofet for technical assistance. E. J.-R. thanks Programa de Becas CONACyT (Número de becario: 837819). Hugo Valdés thanks the Generalitat de Catalunya for a Beatriu de Pinós contract

(grant ID: 2019-BP-0080). The financial support of this research by PAPIIT-DGAPA-UNAM (PAPIIT IN223323), CONACyT A1-S-033933, AEI/MCIU (PID2020-114548 GB-I00, PRE2021-097669), the Generalitat de Catalunya (2021SGR00487), and FEDER (UNGI10-4E-801) is gratefully acknowledged.

Appendix A. Supplementary material

Supplementary data to this article can be found online at <https://doi.org/10.1016/j.jcat.2023.07.001>.

References

- [1] E. Rufino-Felipe, H. Valdés, J.M. Germán-Acacio, V. Reyes-Márquez, D. Morales-Morales, Fluorinated N-Heterocyclic carbene complexes. Applications in catalysis, *J. Organomet. Chem.* 921 (2020).
- [2] H. Valdés, D. Canseco-González, J.M. Germán-Acacio, D. Morales-Morales, Xanthine based N-heterocyclic carbene (NHC) complexes, *J. Organomet. Chem.* 867 (2018) 51–54.
- [3] E. Peris, Smart N-Heterocyclic Carbene Ligands in Catalysis, *Chem. Rev.* 118 (2018) 9988–10031.
- [4] M. Poyatos, J.A. Mata, E. Peris, Complexes with Poly(N-heterocyclic carbene) Ligands: Structural Features and Catalytic Applications, *Chem. Rev.* 109 (2009) 3677–3707.
- [5] J.A. Mata, M. Poyatos, E. Peris, Structural and catalytic properties of chelating bis- and tris-N-heterocyclic carbenes, *Coord. Chem. Rev.* 251 (2007) 841–859.
- [6] S. Díez-González, N. Marion, S.P. Nolan, N-Heterocyclic Carbenes in Late Transition Metal Catalysis, *Chem. Rev.* 109 (2009) 3612–3676.
- [7] J.A. Mata, M. Poyatos, Recent Developments in the Applications of Palladium Complexes Bearing N-Heterocyclic Carbene Ligands, *Curr. Org. Chem.* 15 (2011) 3309–3324.
- [8] C. Valente, S. Çalimsiz, K.H. Hoi, D. Mallik, M. Sayah, M.G. Organ, The Development of Bulky Palladium NHC Complexes for the Most-Challenging Cross-Coupling Reactions, *Angew. Chem. Int. Ed.* 51 (2012) 3314–3332.
- [9] A. Doddi, M. Peters, M. Tamm, N-Heterocyclic Carbene Adducts of Main Group Elements and Their Use as Ligands in Transition Metal Chemistry, *Chem. Rev.* 119 (2019) 6994–7112.
- [10] A.A. Danopoulos, T. Simler, P. Braunstein, N-Heterocyclic Carbene Complexes of Copper, Nickel, and Cobalt, *Chem. Rev.* 119 (2019) 3730–3961.
- [11] G. Sipos, R. Dorta, Iridium complexes with monodentate N-heterocyclic carbene ligands, *Coord. Chem. Rev.* 375 (2018) 13–68.
- [12] Á. Vivancos, C. Segarra, M. Albrecht, Mesoionic and Related Less Heteroatom-Stabilized N-Heterocyclic Carbene Complexes: Synthesis, Catalysis, and Other Applications, *Chem. Rev.* 118 (2018) 9493–9586.
- [13] W. Wang, L. Cui, P. Sun, L. Shi, C. Yue, F. Li, Reusable N-Heterocyclic Carbene Complex Catalysts and Beyond: A Perspective on Recycling Strategies, *Chem. Rev.* 118 (2018) 9843–9929.
- [14] D. Munz, Pushing Electrons—Which Carbene Ligand for Which Application?, *Organometallics* 37 (2018) 275–289.
- [15] E. Peris, Polyaromatic N-heterocyclic carbene ligands and π -stacking. Catalytic consequences, *Chem. Commun.* 52 (2016) 5777–5787.
- [16] V. Ritleng, M. Henrion, M.J. Chetcuti, Nickel N-Heterocyclic Carbene-Catalyzed C-Heteroatom Bond Formation, Reduction, and Oxidation: Reactions and Mechanistic Aspects, *ACS Catalysis* 6 (2) (2016) 890–906.
- [17] E. Levin, E. Ivry, C.E. Diesendruck, N.G. Lemcoff, Water in N-Heterocyclic Carbene-Assisted Catalysis, *Chem. Rev.* 115 (2015) 4607–4692.
- [18] A.P. Prakasham, P. Ghosh, Nickel N-heterocyclic carbene complexes and their utility in homogeneous catalysis, *Inorg. Chim. Acta* 431 (2015) 61–100.
- [19] S. Bellemin-Lapponnaz, S. Dagorne, Group 1 and 2 and Early Transition Metal Complexes Bearing N-Heterocyclic Carbene Ligands: Coordination Chemistry, Reactivity, and Applications, *Chem. Rev.* 114 (2014) 8747–8774.
- [20] M.N. Hopkinson, C. Richter, M. Schedler, F. Glorius, An overview of N-heterocyclic carbenes, *Nature* 510 (2014) 485–496.
- [21] R. Visbal, M.C. Gimeno, N-heterocyclic carbene metal complexes: photoluminescence and applications, *Chem. Soc. Rev.* 43 (10) (2014) 3551–3574.
- [22] J.D. Egbert, C.S.J. Cazin, S.P. Nolan, Copper N-heterocyclic carbene complexes in catalysis, *Cat. Sci. Tech.* 3 (2013) 912–926.
- [23] M. Asay, C. Jones, M. Driess, N-Heterocyclic Carbene Analogues with Low-Valent Group 13 and Group 14 Elements: Syntheses, Structures, and Reactivities of a New Generation of Multitalented Ligands, *Chem. Rev.* 111 (2) (2011) 354–396.
- [24] C. Samojłowicz, M. Bieniek, K. Grela, Ruthenium-Based Olefin Metathesis Catalysts Bearing N-Heterocyclic Carbene Ligands, *Chem. Rev.* 109 (8) (2009) 3708–3742.
- [25] N. Marion, S.P. Nolan, N-Heterocyclic carbenes in gold catalysis, *Chem. Soc. Rev.* 37 (2008) 1776–1782.
- [26] V. César, S. Bellemin-Lapponnaz, L.H. Gade, Chiral N-heterocyclic carbenes as stereodirecting ligands in asymmetric catalysis, *Chem. Soc. Rev.* 33 (2004) 619–636.

- [27] W.A. Herrmann, N-Heterocyclic Carbenes: A New Concept in Organometallic Catalysis, *Angew. Chem. Int. Ed.* 41 (8) (2002) 1290–1309.
- [28] M. Feng, B. Tang, H.S. Liang, X. Jiang, Sulfur Containing Scaffolds in Drugs: Synthesis and Application in Medicinal Chemistry, *Curr. Top. Med. Chem.* 16 (11) (2016) 1200–1216.
- [29] D.A. Boyd, Sulfur and Its Role In Modern Materials Science, *Angew. Chem. Int. Ed.* 55 (2016) 15486–15502.
- [30] G. Evano, C. Theunissen, A. Pradal, Impact of copper-catalyzed cross-coupling reactions in natural product synthesis: the emergence of new retrosynthetic paradigms, *Natural Product Reports* 30 (2013) 1467–1489.
- [31] E.A. Ilardi, E. Vitaku, J.T. Njardarson, Data-Mining for Sulfur and Fluorine: An Evaluation of Pharmaceuticals To Reveal Opportunities for Drug Design and Discovery, *J. Med. Chem.* 57 (7) (2014) 2832–2842.
- [32] Y. Zhang, K.C. Ngeow, J.Y. Ying, The first N-heterocyclic carbene-based nickel catalyst for C-S coupling, *Org. Lett.* 9 (18) (2007) 3495–3498.
- [33] C.-F. Fu, Y.-H. Liu, S.-M. Peng, S.-T. Liu, C-S bond formation catalyzed by N-heterocyclic carbene palladium phosphine complexes, *Tetrahedron* 66 (12) (2010) 2119–2122.
- [34] M.J. Iglesias, A. Prieto, M.C. Nicasio, Well-Defined Allylnickel Chloride/N-Heterocyclic Carbene [(NHC)Ni(allyl)Cl] Complexes as Highly Active Precatalysts for C-N and C-S Cross-Coupling Reactions, *Adv. Synth. Catal.* 352 (11–12) (2010) 1949–1954.
- [35] P. Guan, C. Cao, Y. Liu, Y. Li, P. He, Q. Chen, G. Liu, Y. Shi, Efficient nickel/N-heterocyclic carbene catalyzed C-S cross-coupling, *Tetrahedron Lett.* 53 (45) (2012) 5987–5992.
- [36] G. Bastug, S.P. Nolan, Carbon-Sulfur Bond Formation Catalyzed by [Pd (IPr^oOMe)(cin)Cl] (cin = cinnamyl), *J. Org. Chem.* 78 (18) (2013) 9303–9308.
- [37] H.-J. Yoon, J.-W. Choi, H. Kang, T. Kang, S.-M. Lee, B.-H. Jun, Y.-S. Lee, Recyclable NHC-Ni Complex Immobilized on Magnetite/Silica Nanoparticles for C-S Cross-Coupling of Aryl Halides with Thiols, *Synlett* 2010 (16) (2010) 2518–2522.
- [38] W.-K. Huang, W.-T. Chen, I.J. Hsu, C.-C. Han, S.-G. Shyu, Cross C-S coupling reaction catalyzed by copper(I) N-heterocyclic carbene complexes, *RSC Adv.* 7 (2017) 4912–4920.
- [39] L.B. Junquera, F.E. Fernández, M.C. Puerta, P. Valerga, Nickel(II) N-Heterocyclic Carbene Complexes: Versatile Catalysts for C-C, C-S and C-N Coupling Reactions, *Eur. J. Inorg. Chem.* 2017 (19) (2017) 2547–2556.
- [40] F.-J. Guo, J. Sun, Z.-Q. Xu, F.E. Kühn, S.-L. Zang, M.-D. Zhou, C-S cross-coupling of aryl halides with alkyl thiols catalyzed by in-situ generated nickel(II) N-heterocyclic carbene complexes, *Catal. Commun.* 96 (2017) 11–14.
- [41] M.A. Rodríguez-Cruz, S. Hernández-Ortega, H. Valdés, E. Rufino-Felipe, D. Morales-Morales, C-S cross-coupling catalyzed by a series of easily accessible, well defined Ni(II) complexes of the type [(NHC)Ni(Cp)(Br)], *J. Catal.* 383 (2020) 193–198.
- [42] E. Rufino-Felipe, H. Valdés, D. Morales-Morales, C-S Cross-Coupling Reactions Catalyzed by Well-Defined Copper and Nickel Complexes, *Eur. J. Org. Chem.* 2022 (2022) e202200654.
- [43] H.V. Huynh, Electronic Properties of N-Heterocyclic Carbenes and Their Experimental Determination, *Chem. Rev.* 118 (2018) 9457–9492.
- [44] D.J. Nelson, S.P. Nolan, Quantifying and understanding the electronic properties of N-heterocyclic carbenes, *Chem. Soc. Rev.* 42 (2013) 6723–6753.
- [45] H. Valdés, M. Poyatos, G. Ujaque, E. Peris, Experimental and theoretical approaches to the influence of the addition of pyrene to a series of Pd and Ni NHC-based complexes: Catalytic consequences, *Chem. Eur. J.* 21 (4) (2015) 1578–1588.
- [46] A.G. Gökçe, S. Gülcemal, M. Aygün, B. Çetinkaya, O. Büyükgüngör, trans-Bis[1-benzyl-3-(2,3,4,5,6-pentafluorobenzyl)benzimidazol-2-ylidene]dibromopalladium(II), *Acta Cryst. C* 62 (11) (2006) m535–m537.
- [47] S. Díez-González, S.P. Nolan, Stereoelectronic parameters associated with N-heterocyclic carbene (NHC) ligands: A quest for understanding, *Coord. Chem. Rev.* 251 (5–6) (2007) 874–883.
- [48] R. Rubbiani, I. Kitanovic, H. Alborzina, S. Can, A. Kitanovic, L.A. Onambele, M. Stefanopoulou, Y. Geldmacher, W.S. Sheldrick, G. Wolber, A. Prokop, S. Wölfl, I. Ott, Benzimidazol-2-ylidene Gold(I) Complexes Are Thioresoxin Reductase Inhibitors with Multiple Antitumor Properties, *J. Med. Chem.* 53 (2010) 8608–8618.
- [49] Bruker 2018. Programas: APEX3, SAINT, Bruker AXS Inc., Madison, Wisconsin, USA.
- [50] G. Sheldrick, Crystal structure refinement with SHELXL, *Acta Cryst. C* 71 (2015) 3–8.
- [51] L. Krause, R. Herbst-Irmer, G.M. Sheldrick, D. Stalke, Comparison of silver and molybdenum microfocus X-ray sources for single-crystal structure determination, *J. Appl. Crystallogr.* 48 (2015) 3–10.
- [52] M. Güell, J.M. Luis, M. Solà, M. Swart, Importance of the Basis Set for the Spin-State Energetics of Iron Complexes, *J. Phys. Chem. A* 112 (2008) 6384–6391.
- [53] E. Van Lenthe, E.J. Baerends, Optimized Slater-type basis sets for the elements 1–118, *J. Comput. Chem.* 24 (2003) 1142–1156.
- [54] M. Swart, A new family of hybrid density functionals, *Chem. Phys. Lett.* 580 (2013) 166–171.
- [55] P. Pirovano, E.R. Farquhar, M. Swart, A.J. Fitzpatrick, G.G. Morgan, A.R. McDonald, Characterization and Reactivity of a Terminal Nickel(III)-Oxygen Adduct, *Chem. Eur. J.* 21 (2015) 3785–3790.
- [56] S.K. Padamati, D. Angelone, A. Draksharapu, G. Primi, D.J. Martin, M. Tromp, M. Swart, W.R. Browne, Transient Formation and Reactivity of a High-Valent Nickel(IV) Oxido Complex, *J. Am. Chem. Soc.* 139 (2017) 8718–8724.
- [57] M.D. Wilkinson, M. Dumontier, I.J. Aalbersberg, G. Appleton, M. Axton, A. Baak, N. Blomberg, J.-W. Boiten, L.B. da Silva Santos, P.E. Bourne, J. Bouwman, A.J. Brookes, T. Clark, M. Crosas, I. Dillo, O. Dumon, S. Edmunds, C.T. Evelo, R. Finkers, A. Gonzalez-Beltran, A.J.G. Gray, P. Groth, C. Goble, J.S. Grethe, J. Heringa, P.A.C. 't Hoen, R. Hooft, T. Kuhn, R. Kok, J. Kok, S.J. Lusher, M.E. Martone, A. Mons, A.L. Packer, B. Persson, P. Rocca-Serra, M. Roos, R. van Schaik, S.-A. Sansone, E. Schultes, T. Sengstag, T. Slater, G. Strawn, M.A. Swertz, M. Thompson, J. van der Lei, E. van Mulligen, J. Velterop, A. Waagmeester, P. Wittenburg, K. Wolstencroft, J. Zhao, B. Mons, The FAIR Guiding Principles for scientific data management and stewardship, *Sci. Data* 3 (2016) 160018.